Branching ratios of autoionization from Eu $4f^7 6p_{1/2} 6d\,[J]$ autoionizing states*

Yan Jun-Gang(闫俊刚)[a)b)], Shen Li(沈 礼)[a)b)], Liang Hong-Rui(梁洪瑞)[a)b)], and Dai Chang-Jian(戴长建)[a)b)†]

[a)] *Key Laboratory of Display Materials and Photoelectric Devices, Ministry of Education, Tianjin* 300384, *China*

[b)] *School of Science, Tianjin University of Technology, Tianjin* 300384, *China*

(Received 4 January 2015; revised manuscript received 3 March 2015; published online 20 June 2015)

The autoionization branching ratios from Eu $4f^7 6p_{1/2} 6d\,[J]$ autoionizing states to its $4f^7 6s^+$ ($^9S^o$), $4f^7 6s^+$ ($^7S^o$), and $4f^7 5d^+$ ($^9D^o$) final ionic states are investigated with the combination of the three-step laser excitation and the velocity-map imaging technique. These different autoionizing states are excited via $4f^7 6s6d\ ^8D_J$ [$J = 5/2$, 7/2, and 9/2] intermediate states, respectively. The experimental photoelectron images are obtained, from which energy distributions of ejected electrons are achieved with the mathematical transformation. Furthermore, the energy dependence of the branching ratio is investigated within the autoionization resonance, by which population inversion is observed as an important characteristic. The J-dependence is also studied systematically. The validity of the well-known isolated core excitation technique used for obtaining the autoionization spectrum is also studied.

Keywords: Eu atom, velocity-map imaging, autoionizing state, autoionization branching ratio

PACS: 32.80.Zb, 32.30.–r, 32.80.Ee **DOI:** 10.1088/1674-1056/24/8/083203

1. Introduction

As is well known, an autoionization spectrum only represents the total cross section of the autoionization process, while the branching ratio (BR) of autoionization may provide more detailed information about the autoionization process, such as its final ionic states and its ratios for different decay paths. Thus, the study on the BR of autoionization process may not only enrich the knowledge about the autoionizing state of the complex atomic system, but also explore its dynamical characteristics of the autoionization process.

During the last few decades, both total cross sections[1–3] and partial cross sections[4,5] of autoionization for several alkaline-earth atoms have been investigated, approaching perfection in the study of autoionization of alkaline-earth atoms. Meanwhile, studies on both bound and autoionizing states of rare-earth atoms have been reported.[6–12] However, less attention has been paid to the BR of autoionization,[13] making it necessary for us to explore the BR of autoionization for the rare-earth Eu atom.

Traditionally, the distributions of kinetic energy of ejected electrons are measured by the time of flight (TOF) technique, which needs a long drift tube. Due to the very small solid angle of acceptance for an electron, the BR signal is very weak, leading to a very poor signal-to-noise ratio (SNR).[14] Recently, a newly developed velocity-map imaging (VMI) technique has been developed to avoid this difficulty by focusing all ejected electrons onto the detector with a set of electron lenses,[15] which has been demonstrated in studying dynamical process of atomic and molecular systems.[16,17]

Based on the above facts, a recent study expanded the application of the VMI technique to the BR of autoionization from Eu $4f^7 6p_{1/2} 8s$ autoionizing state,[13] which is a member of the $6p_{1/2}\ ns$ Rydberg series. However, no work on the Eu $6p_{1/2}\ nd$ Rydberg series has been reported so far, which is curious to anybody in this field. Thus, studying Eu $4f^7 6p_{1/2} 6d$ autoionizing states allows us to take the next step towards exploring the BR of autoionization for the Eu atom: first, unlike Eu $4f^7 6p_{1/2} 8s$ autoionizing Rydberg states, the $4f^7 6p_{1/2} 6d$ autoionizing states are the lowest members of $6p_{1/2}\ nd$ autoionizing series, which are the best candidates to test the validity of the well-known isolated core excitation (ICE) technique. This configuration interaction between $4f^7 6p_{1/2} 6d$ autoionizing states and $4f^7 5d$ ($^7D^o$) nl states may lead to complex structures of the autoionization spectra of $4f^7 6p_{1/2} 6d$ and complex variation of BR of autoionization from the $4f^7 6p_{1/2} 6d$ autoionizing states. From the above description, it is indispensable to explore the BR of autoionization from $4f^7 6p_{1/2} 6d$ autoionizing states.

The experimental setup and approach are stated in Section 2, while the analysis of results is provided in Section 3. Finally, the conclusion is given in the last section.

2. Experiment setup and methods

2.1. Experiment setup

As shown in Fig. 1, the setup used in this work contains a high energy laser system, an Eu atomic beam production sys-

*Project supported by the National Natural Science Foundation of China (Grant No. 11174218).

†Corresponding author. E-mail: daicj@126.com

© 2015 Chinese Physical Society and IOP Publishing Ltd

tem and a signal collecting system. Since a detailed description of the experimental setup can be found in Ref. [13], only a brief introduction is given here.

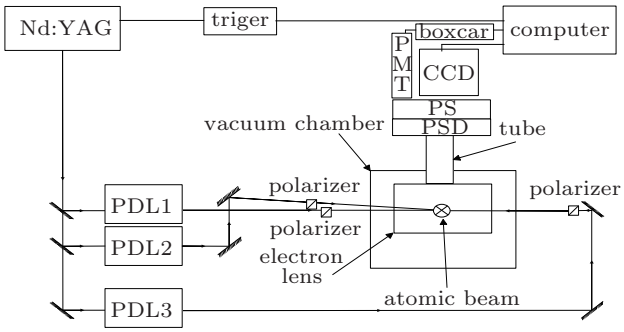


Fig. 1. Experimental setup including a high energy laser system, an Eu atomic beam production system, and a signal collecting system.

The high energy laser system contains three tunable dye lasers each with a line width of 0.2 cm^{-1} and pulse energy of 0.5 mJ pumped by the 2nd-harmonic or the 3rd-harmonic generation of the same high energy pulsed Nd:YAG laser at wavelengths of 532 nm and 355 nm with a pulse duration of 6 ns–8 ns, running at 20 Hz.

The Eu atomic beam production system, inside a vacuum chamber with a typical pressure of about 10^{-5} Pa, generates an effusive atomic beam with continuous heating from an oven. To reduce the Doppler broadening, the atomic beam is crossed perpendicularly with dye laser beams in the interaction region.

The signal collecting system mainly includes an electron lens, a position sensitive detector (PSD), phosphor screen (PS), and charge coupled device (CCD). Electrons ejected from autoionization are imaged on the PSD, then, the fluorescence signal from the PS is obtained by a CCD and delivered to a computer for further analysis.

2.2. Methods

In order to populate the $4f^7 6p_{1/2} 6d$ [J] autoionizing states with different values of total angular momentum J, the following three excitation schemes are employed:

Scheme I:

$$4f^7 6s^2 {}^8S_{7/2} \xrightarrow{\lambda_1} 4f^7 6s6p {}^8P_{7/2} \xrightarrow{\lambda_2} 4f^7 6s6d {}^8D_{9/2} \xrightarrow{\text{scan } \lambda_3} 4f^7 6p_{1/2} 6d\ [J = 7/2, 9/2, \text{ or } 11/2,$$

Scheme II:

$$4f^7 6s^2 {}^8S_{7/2} \xrightarrow{\lambda_1} 4f^7 6s6p {}^8P_{7/2} \xrightarrow{\lambda_2} 4f^7 6s6d {}^8D_{7/2} \xrightarrow{\text{scan } \lambda_3} 4f^7 6p_{1/2} 6d\ [J = 5/2, 7/2, \text{ or } 9/2,$$

Scheme III:

$$4f^7 6s^2 {}^8S_{7/2} \xrightarrow{\lambda_1} 4f^7 6s6p {}^8P_{7/2} \xrightarrow{\lambda_2} 4f^7 6s6d {}^8D_{5/2} \xrightarrow{\text{scan } \lambda_3} 4f^7 6p_{1/2} 6d\ [J = 3/2, 5/2, \text{ or } 7/2],$$

where λ_1 is fixed at 462.71 nm, and λ_2 is fixed at different wavelengths to excite the three different $4f^7 6s6d$ states respectively, while the third laser is then scanned to drive the $4f^7 6s^+ \rightarrow 4f^7 6p^+_{1/2}$ transition. With the above stepwise excitations, photons from three linearly polarized lasers interact with the Eu atom. To make the processes more evident, the above excitation schemes are also shown in Fig. 2.

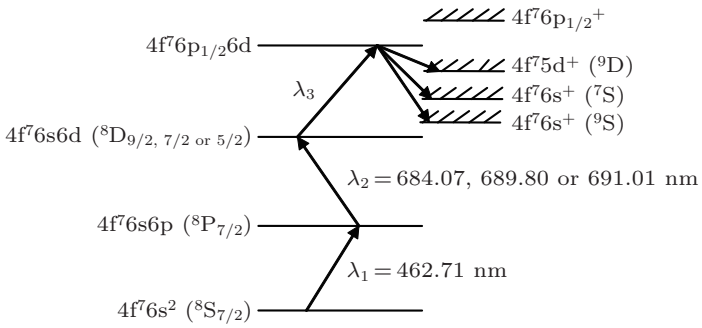


Fig. 2. Diagram of several excitation schemes. λ_1 is fixed at 462.71 nm, and λ_2 is fixed at 684.07 nm, 689.80 nm, or 691.01 nm to populate several different $4f^7 6s6d$ (^{8}D) Rydberg states respectively, while λ_3 is scanned to populate the $4f^7 6p_{1/2} 6d$ autoionizing states.

As shown in Fig. 2, the $4f^7 6p_{1/2} 6d$ autoionizing states are excited from several different $4f^7 6s6d$ states, which are excited from the $4f^7 6s^2$ ($^8S^o$) ground state via the $4f^7 6s6p$ intermediate state. The Eu atom in the autoionizing states may decay to the $4f^7 6s^+$ ($^9S^o$), $4f^7 6s^+$ ($^7S^o$), and $4f^7 5d^+$ ($^9D^o$) ionic states, respectively.

In the present experiment, the energy distribution (ED) of electrons ejected from autoionization is observed and analyzed in order to obtain the information for the possible ionic final states. Specifically, energy conservation of the autoionization process results in the one-to-one correspondence between the ejected electron and the ion in the above final state. To obtain the BR of the ejected electron from the autoionization, the inverted Abel transformation is used to recover the three-dimensional (3D) velocity distribution from the two-dimensional (2D) projection image of the ejected electron measured by the CCD.

To obtain the ED of electrons ejected from autoionization, several parameters of VMI need to be adjusted. First, to ensure that the ejected electrons with different kinetic energies are located accurately, it is necessary to calibrate the spatial location of the image with VMI. Namely, the electrons ejected from a direct photoionization to the continuum state can be used as a sample with zero kinetic energy, which can be adjusted to be the center of the projection image. Second, in order to have a sufficient contrast and resolution between the bright and dark rings in the image, it is important to scale the intensity of the image with the VMI. The BASEX software is used to reconstruct the 3D distribution through the Abel inversion transformation. The 3D velocity distribution can be

further processed by an angular integral to obtain the partial populations of the respective final states. In this experiment, the quality of VMI image is determined mainly by the CCD, which has a resolution of 1024×1024 pixels, and a pixel area of 13 μm×13 μm.

The uncertainties of the experiment originate from the alignments of both the VMI detector geometry and the electron lens assembly with respect to the axis of the PSD, which may cause distortions in the images far from the center of the PSD. Meanwhile, the brightness calibration of the VMI image may lead to the uncertainty in boundaries within which angular integral is undertaken. The overall uncertainty is estimated to be 5% in the ED of electrons ejected from autoionization.

3. Results and discussion

In order to discuss the results of autoionization BR, and to explore any differences among the three different $4f^7 6p_{1/2} 6d$ autoionizing states in terms of the BR, it is necessary to identify their autoionization spectra first.

3.1. $4f^7 6p_{1/2} 6d$ autoionization spectra

Since the $4f^7 6p_{1/2} 6d$ [J] autoionizing states are so low that they are also below the $4f^7 5d^+$ ($^7D^o$) ionization limit, the possible configuration interaction between these series, $4f^7 6p_{1/2} 6d$ [J] and $4f^7 5d$ ($^7D^o$) nl, is expected. The three spectra of $4f^7 6p_{1/2} 6d$ [J] autoionizing states are shown in Fig. 3.

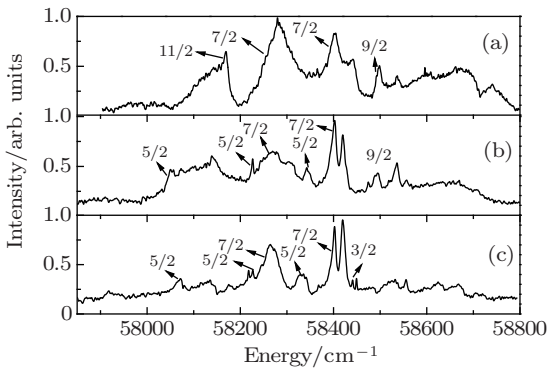


Fig. 3. Experimental spectra of $4f^7 6p_{1/2} 6d$ autoionizing states in the energy range 57900 cm^{-1}–58900 cm^{-1}. (a) $4f^7 6p_{1/2} 6d$ [$J = 7/2$, 9/2 or 11/2] spectra; (b) $4f^7 6p_{1/2} 6d$ [$J = 5/2$, 7/2 or 9/2] spectra, (c) $4f^7 6p_{1/2} 6d$ [$J = 3/2$, 5/2 or 7/2] spectra, obtained with schemes I, II, and III, respectively.

As shown in Fig. 3, the three spectra of $4f^7 6p_{1/2} 6d$ [J] autoionizing states are all superimposed with some narrow peaks, which are considered as the fingerprints of $4f^7 5d$ ($^7D^o$) nl states. Furthermore, based on the selection rules ($\Delta J = 0$, ± 1) of the three excitation schemes described in Section 2, all the features in the three spectra can be identified uniquely. These identifications can be made by making a comparison of these spectra, and denoting the peaks with $J = 9/2$, 7/2 or 5/2, respectively as shown in Fig. 3. In order to observe the J-dependence of the BR, the energy and J-assignment of the peaks are listed in the Table 1.

Table 1. Energies and J-assignments of the peaks.

Peak number	Energy/cm^{-1}	Scheme	J
1	58060.5	II, III	5/2
2	58169.9	I	11/2
3	58227.6	II, III	5/2
4	58270.8	I, II, III	7/2
5	58340.2	II, III	5/2
6	58401.6	I, II, III	7/2
7	58440.7	III	3/2
8	58496.8	I, II	9/2

Turning now to the line shapes of the $4f^7 6p_{1/2} 6d$ autoionizing states, which are the lowest members of $4f^7 6p_{1/2}$ nd autoionizing series, and the best candidates to test the validity of the well-known isolated core excitation (ICE) technique. As a powerful three-step excitation method, the ICE scheme has been used extensively to study the autoionizing states of alkaline-earth atoms[18,19] and rare-earth atoms.[20,21] For instance, the autoionization spectra of the Ba $6p_{1/2}$ nd states, with $n = 7$–15, exhibit the Lorentzian profiles.[18] This is understandable, because for the higher-n $6p_{1/2}$ nd autoionizing states, the nd Rydberg electron is too far from the core, which is isolated during the $6s^+ \rightarrow 6p^+_{1/2}$ excitation. However, this may not be the case for the Eu $4f^7 6p_{1/2} 6d$ autoionizing states, since the 6d electron is even closer to the core.

Based on the above analysis, it is very interesting to see whether there is a difference between the Ba $6p_{1/2} 7d$ and Eu $4f^7 6p_{1/2} 6d$ autoionizing states in terms of their line shapes. Specifically, we attempt to find the limit of n where the ICE scheme is still valid for the Eu $4f^7 6p_{1/2} 6d$ autoionizing states, which are the best candidates for testing the validity of the ICE scheme. As shown in Fig. 3, all three autoionization spectra exhibit the Fano-type line shapes, instead of the Lorentzian type, manifesting an interference effect between the two excitation paths during the third-step excitation. This phenomenon indicates that the core is by no means isolated during the $4f^7 6s^+ \rightarrow 4f^7 6p^+_{1/2}$ excitation, as the 6d Rydberg electron is too close to it. Namely, the excitations of the 6d$\rightarrow$ εp, εf continuum states are accompanied by the $4f^7 6s^+ \rightarrow 4f^7 6p^+_{1/2}$ excitation in the third-step excitation, leading to their competition of absorbing the photons from the third-step laser. The simultaneous excitations of the two channels, to the $4f^7 6p_{1/2} 6d$ autoionizing states and to the $4f^7 6s$ εp, εf continuum states, induce the interference effect between them, resulting in the Fano-type line shapes. Due to the violation of the ICE scheme, the advantage of the technique partially vanishes, which means the ICE scheme is only valid down to the $n = 7$ state, which was confirmed by the experiments on the Ba[18] and Sm[21] atoms. The invalidity of the ICE scheme for the $n = 6$ state

is an important limit to experimental studies of autoionizing states.

All the characteristics discussed above have manifested a comprehensive configuration interaction among the different autoionization series, which may have a significant influence on the autoionization process. Thus, the possible influence on the autoionization BR will be expected, which is described in the next subsection.

3.2. Branching ratio of autoionization

As pointed out earlier, an autoionization spectrum represents the total cross section of the autoionization process, while the autoionization BR to final ionic states corresponds to the partial cross section of the same process. Thus, autoionization spectra of $4f^7 6p_{1/2} 6d$ states themselves provide no information about possible final ionic states, including their number and the BR, while the ED of electrons ejected from autoionization needs to be explored. In other words, to know how many ionic states are involved and what the percentages of ions among them are, we should observe the ejected electrons from autoionization.

To carry out such an experiment, the VMI technique is employed to obtain the images of ejected electrons from the autoionization process, an example of which is shown in Fig. 4. At a fixed energy, the ED of ejected electrons from the $4f^7 6p_{1/2} 6d$ autoionizing state can be extracted from fitting the Abel-inverted images.

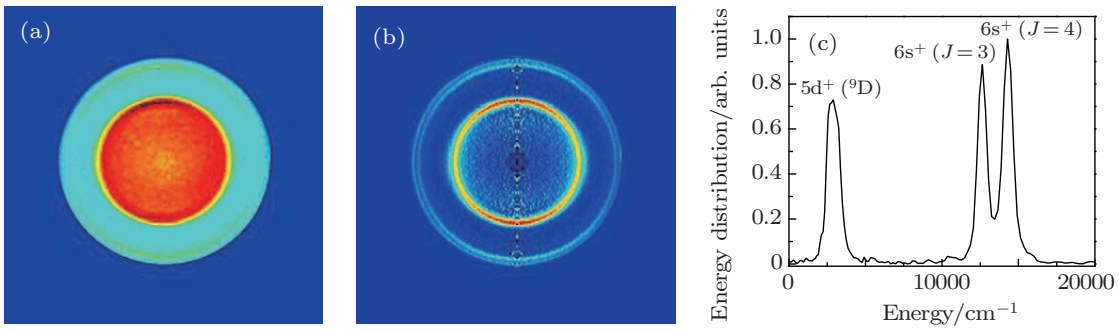


Fig. 4. (color online) The VMI image and the ED spectrum at the fixed energy of the $4f^7 6p_{1/2} 6d$ state. The original image (a), the Abel-inverted image (b), and the ED of ejected electron (c) to the final ion states are illustrated.

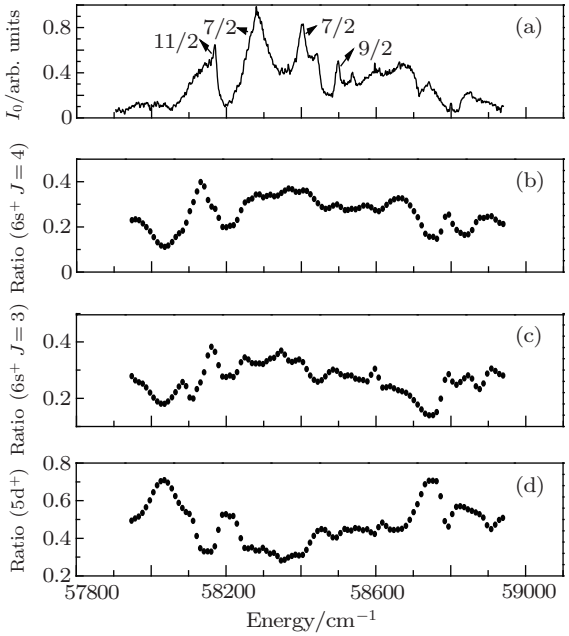


Fig. 5. Autoionization BR and spectra of the $4f^7 6p_{1/2} 6d$ [$J = 7/2$, 9/2 or 11/2] state. (a) Spectrum, (b) BR_1, (c) BR_2, and (d) BR_3.

As shown in Fig. 4, the fine structures of the $4f^7 5d^+$ ($^9D^o$) ionic states cannot be resolved, while the two ionic states, $6s^+$ ($^9S^o$) and $6s^+$ ($^7S^o$), can be resolved. There are three autoionization channels: $4f^7 6p_{1/2} 6d \rightarrow (4f^7 6s^{+9}S^o J = 4) + e^-(\varepsilon l)$, $4f^7 6p_{1/2} 6d \rightarrow (4f^7 6s^{+7}S^o J = 3) + e^-(\varepsilon l)$, and $4f^7 6p_{1/2} 6d \rightarrow (4f^7 5d^{+9}D^o) + e^-(\varepsilon l)$, where ε represents the energy of ejected electron and l denotes the orbital angular momentum.

Meanwhile, the BR can be extracted from Fig. 4(c) based on the areas under the different profiles. Let BR_1, BR_2, and BR_3 be the BRs to the $6s^+$ ($^9S^o$), $6s^+$ ($^7S^o$), and $5d^+$ ($^9D^o$) ionic states, respectively, then the calculation yields $BR_1 = 33.4\%$, $BR_2 = 29.6\%$, and $BR_3 = 37.0\%$.

In order to explore the energy dependence of BR, the third-step laser is scanned within the spectra of the $4f^7 6p_{1/2} 6d$ states. An example is shown in Fig. 5, for the spectrum and three BR_i ($i = 1$–3) of the $4f^7 6p_{1/2} 6d$ [$J = 7/2$, 9/2 or 11/2] states.

As seen in Fig. 5, the BR_3 is much larger than BR_1 or BR_2, meaning that the Eu atom mainly autoionizes to the $4f^7 5d^+$ ($^9D^o$) ionic state in almost the whole energy region. More interestingly, nearly 70% of Eu atoms will autoionize to the $4f^7 5d^+$ ($^9D^o$) ionic state, leading to a population inversion, which is significant for developing an ion laser, just like the Ba^+ laser based on autoionization.[22,23]

Meanwhile, all peaks in the spectra of BRs seem to have no correspondence to those in the autoionization spectrum, which can be partially attributed to the interaction between the

$4f^7 6p_{1/2} 6d$ [J] and $4f^7 5d$ ($^7D^o$) nl autoionizing states in the same energy region.

However, with the aid of Table 1, the J-dependence can be found if we take a closer look at Fig. 5. For instance, in the region around the peak with $J = 11/2$ in Fig. 5(a), both the BR_1 and BR_2 decrease remarkably, while the BR_3 increases rapidly, as opposed to the regions where the peaks with $J = 7/2$ or 9/2 are located, in which the BRs vary gently.

Another example is shown in Fig. 6 for the $4f^7 6p_{1/2} 6d$ [$J = 5/2$, 7/2 or 9/2] autoionizing state, which is obtained with different paths from those of Fig. 5.

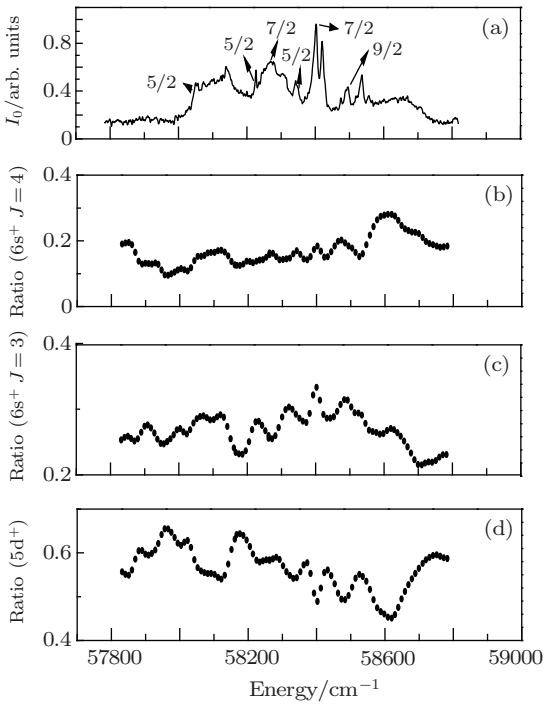


Fig. 6. Autoionization BR and spectra of $4f^7 6p_{1/2} 6d$ [$J = 5/2$, 7/2 or 9/2] state. (a) Spectrum, (b) BR_1, (c) BR_2, and (d) BR_3.

What can be seen from Fig. 6 is similar to the case shown in Fig. 5, where population inversion is still kept for most of the time. The BRs of $4f^7 6p_{1/2} 6d$ [$J = 5/2$, 7/2 or 9/2] autoionizing states to $4f^7 6s^+$ ($^9S^o$), $4f^7 6s^+$ ($^7S^o$), and $4f^7 5d^+$ ($^9D^o$) ionic states, are fluctuated from 21% to 33%, 9% to 28%, and 45% to 65%, respectively. Furthermore, a similar trend of BR variation to the J value is also revealed from Fig. 6. For example, in the region around the peak with $J = 7/2$ on the left side, the BRs are still varied gently. However, we do find several differences between Figs. 5 and 6. Namely, the BRs vary remarkably in the two regions, corresponding to the peak with $J = 7/2$ on the right side, and the one with $J = 9/2$ in Fig. 6, while the same is not true in Fig. 5.

The last example of the series experiments is shown in Fig. 7 for $4f^7 6p_{1/2} 6d$ [$J = 3/2$, 5/2 or 7/2] autoionizing state, to be compared with those shown in Figs. 5 and 6.

As seen in Fig. 7, in the region around the two peaks with $J = 11/2$, the BRs are similar to the case in Fig. 6, while they hardly vary in all other regions where the $J = 5/2$ and 3/2 peaks are located.

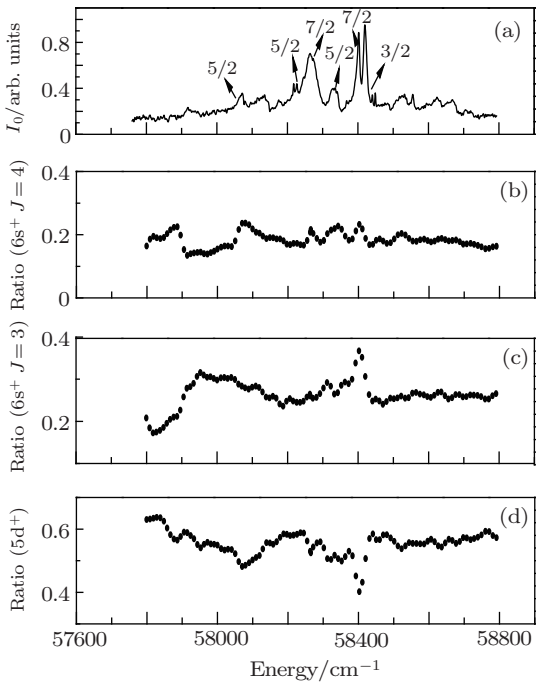


Fig. 7. Autoionization BR and spectra of $4f^7 6p_{1/2} 6d$ [$J = 3/2$, 5/2 or 7/2] state. (a) Spectrum, (b) BR_1, (c) BR_2, and (d) BR_3.

Finally, we make a comment by inspecting all the spectra shown in Figs. 5 and 6. Apart from some exceptions, most variations in the spectra of BRs seem to have no correspondence to those in autoionization spectra, which can be again partially attributed to the interaction between $4f^7 6p_{1/2} 6d$ [J] and $4f^7 5d$ ($^7D^o$) n$l$autoionizing states in the same energy region.

4. Conclusions

The branching ratios of autoionization from $4f^7 6p_{1/2} 6d$ autoionizing states to $4f^7 6s^+$ ($^9S^o$), $4f^7 6s^+$ ($^7S^o$), and $4f^7 5d^+$ ($^9D^o$) ionic states are investigated comprehensively. Although the branching ratios of the three states can be resolved and analyzed with the velocity-map-imaging technique, the fine-structures of $4f^7 5d^+$ ($^9D^o$) state fail to be resolved in the measurement. Both the autoionization spectra and the branching ratios for $4f^7 6p_{1/2} 6d$ autoionizing states manifest the heavy configuration interaction between $4f^7 6p_{1/2} 6d$ and the $4f^7 5d$ nl autoionization series.

The energy dependence and variation with the J value are also studied systematically. It is found that the $4f^7 6p_{1/2} 6d$ states mainly autoionize into the $4f^7 5d^+$ ($^9D^o$) ion states, leading to a population inversion, which is significant for developing an autoionization laser. Furthermore, the validity of the well-known isolated core excitation technique used for obtaining the Lorentzian-type of autoionization spectra is also studied.

References

[1] Jones R R, Dai C J and Gallagher T F 1990 *Phys. Rev. A* **41** 316
[2] Lindsay M D, Dai C J, Lyons B J, Mahon C R and Gallagher T F 1994 *Phys. Rev. A* **50** 5058
[3] Dai C J 1995 *Phys. Rev. A* **52** 4416
[4] Lindsay M D and Dai C J 1992 *Phys. Rev. A* **46** 3789
[5] Zhang Y and Dai C J 2003 *Journal of Electron Spectroscopy* **128** 135
[6] Bushaw B A, Nortershauser W, Blaum K and Wendtd K 2003 *Spectrochim Acta Part B* **58** 1083
[7] Gou B C and Zhu J J 2009 *Acta Phys. Sin.* **58** 5285 (in Chinese)
[8] Bhattacharyya S, Souza R D, Rao P M and Razvi M A N 2003 *Spectrochim Acta Part B* **58** 469
[9] Gou B C, Zhuo L and Wu X L 2010 *Chin. Phys. Lett.* **27** 043101
[10] Bhattacharyya S, Nakhate S G, Jayasekharan T and Razvi M A N 2006 *Phys. Rev. A* **73** 2506
[11] Yang L, Dai C J and Zhao Y H 2013 *Acta Phys. Sin.* **62** 053201 (in Chinese)
[12] Wang X, Shen L and Dai C J 2012 *J. Phys. B: At. Mol. Opt. Phys.* **45** 5001
[13] Liang H R, Shen L, Jing H and Dai C J 2014 *Acta Phys. Sin.* **63** 133202 (in Chinese)
[14] Kachru R, van Linden, van den Heuvell H B and Gallagher T F 1985 *Phys. Rev. A* **31** 700
[15] Keeffe P O, Bolognesi P, Richter R, Moise A, Ovcharenko Y, King G C and Avaldi L 2011 *Phys. Rev. A* **84** 025404
[16] Stodolna A S, Rouzee A, Lepine F, Cohen S, Robicheaux F, Gijsbertsen A, Jungmann J H, Bordas C and Vrakking M J J 2013 *Phys. Rev. Lett.* **110** 3001
[17] Goto M and Hansen K 2012 *Phys. Scr.* **86** 035303
[18] Yuan W G, Dai C J, Jin S, Zhao H Y and Guan F 2008 *Acta Phys. Sin.* **57** 4076 (in Chinese)
[19] Li S B and Dai C J 2007 *Chin. Phys.* **16** 382
[20] Xiao Y, Dai C J and Qin W J 2009 *Chin. Phys. B* **18** 4251
[21] Zhao Y H, Dai C J and Ye S W 2013 *Chin. Phys. B* **22** 023203
[22] Bokor J, Freeman R R and Cooke W E 1982 *Phys. Rev. Lett.* **48** 1242
[23] Freeman R R, Bokor J and Cooke W E 1982 *Phys. Rev. A* **26** 3029